PTEN loss in glioma cell lines leads to increased extracellular vesicle biogenesis and PD-L1 cargo in a PI3K-dependent manner

Authors: Julio C. Sanchez[1], Timothy M. Pierpont[2], Dariana Argueta-Zamora[1], Kristin Wilson[1], Avery August[2], Richard A. Cerione[1,3]

1. Department of Molecular Medicine, College of Veterinary Medicine, Cornell University, Ithaca, NY, 14853, USA
2. Department of Microbiology and Immunology, College of Veterinary Medicine, Cornell University, Ithaca, NY, 14853, USA
3. Department of Chemistry and Chemical Biology, Cornell University, Ithaca, NY, 14853, USA

Abstract

Phosphatase and Tensin Homologue (PTEN) is one of the most frequently lost tumor suppressors in cancer and the predominant negative regulator of the PI3K/AKT signaling axis. A growing body of evidence has highlighted the loss of PTEN with immuno-modulatory functions including the upregulation of the programmed death ligand-1 (PD-L1) and the development of an immunosuppressive tumor immune microenvironment (TIME), which is most likely the result of an altered secretome. Given their roles in immunosuppression and tumor growth, this raises the question of how the loss of PTEN impacts the biogenesis and function of extracellular vesicles (EVs). Here we show that the loss of this tumor suppressor in glioma cells is accompanied by an enhanced ability to produce EVs enriched with PD-L1 that is largely dependent on PI3K activity. We further show that EVs derived from glioma cells lacking PTEN have a greater ability to suppress T cell receptor (TCR) signaling in response to IFN-γ. Taken together, these findings provide important new insights into how the loss of PTEN can contribute to immune evasion and highlights a role for PI3K as a novel regulator of EV biogenesis and the cargo they contain.

Introduction

Primary glioblastoma multiforme (GBM) is classified as a grade IV astrocytoma by the World Health Organization and is the most common and aggressive CNS-related tumor diagnosed, with a mean survival time ranging between 12-18 months.[1] Only 6-12% of patients reach a five-year survival rate, and during the past several years there have not been significant changes in the standard of care[2]. Therefore, there remains a great need to bring new strategies to bear on this devastating disease. The advent of novel immunotherapies such as immune checkpoint inhibitors (ICIs) has

shown a great deal of success against certain forms of cancer by successfully treating otherwise terminally ill patients.[3] ICIs are monoclonal antibodies that block the interaction between immunosuppressive ligands, typically expressed by tumor or myeloid cells, and their cognate checkpoint receptors expressed on T cells. For example, blocking the interaction between the programmed death protein 1 (PD-1) receptor and its ligand (PD-L1) allows for adequate T cell receptor (TCR) activation and thus anti-tumor cytotoxic T cell functions to manifest[3]. For this reason, studies elucidating how PD-L1 and other immunosuppressive ligands are regulated at the cellular level have generated a great deal of attention. We now know that cancer cells upregulate PD-L1 expression in response to inflammatory cytokines such as interferon-γ (IFN-γ), in a process known as "adaptive immune resistance," and can be predictive of successful patient response rates to ICI.[4,5] However, while ICIs have led to robust response rates in select tumor types such as melanoma and NSCLC, the majority of solid tumor-bearing patients, including those diagnosed with GBM have thus far experienced little benefit from these therapies.[6–8] Recent clinical reports have associated the loss of PTEN as a significant biomarker for patients who fail to respond to ICIs across several tumor types including those arising from GBM, melanoma, as well as gastrointestinal and breast cancers.[9–12] PTEN is one of the most frequently deleted tumor suppressors across all cancers,[13,14] with 40-60% of GBM patients exhibiting such deletions.[15] Therefore, understanding how the loss of PTEN impacts the tumor immune microenvironment (TIME), immune evasion, and contribution towards ICI resistance, represent critically important questions.

PTEN is predominantly recognized as the primary lipid phosphatase responsible for reverting the class I PI3K-generated lipid second messenger, phosphatidylinositol (3,4,5)-triphosphate (PIP_3), to

phosphatidylinositol (4,5)-diphosphate (PIP_2).[16] The loss of PTEN and/or hyperactivating mutations associated with PI3K lead to elevated levels of PIP_3 and increased activation of important pleckstrin homology (PH) containing protein kinases such as PDK1, AKT, and mTORC2. Together, these protein kinases activate many of the oncogenic signaling pathways that give rise to enhanced cell growth, survival, metabolic changes and cell migration.[17–19] While loss of PTEN is most recognized for promoting these gain-of-function signaling outcomes, a growing body of evidence suggests that loss or impairment of PTEN function and the accompanying increase in PI3K activity contribute to immune evasion and to the formation of an immunosuppressive TIME.[20–23] As a result, tumors lacking PTEN are more likely to be considered immunologically "cold," showing little or no tumor infiltrating lymphocytes (TILs) while consisting of immunosuppressive and pro-tumorigenic myeloid and lymphoid cells.[24–26] These observations further suggest that the loss of PTEN may have an influence on the ability of tumor cells to communicate with their immediate environment. Along these lines, it has been suggested that the loss of PTEN can impact the secretome of cancer cells, including chemokines and cytokines that aid in the intravasation and reprogramming of lymphoid and myeloid cells into protumor-genic and immunosuppressive cell types.[27–29] These findings thus prompted the question of whether the loss of PTEN and/or hyperactive PI3K signaling might affect the biogenesis and/or the cargo of extracellular vesicles (EVs), which represent another major component of the cancer cell secretome.

EVs are a group of secretory vesicles that play important roles in intercellular communication in a wide range of biology and disease by means of receptor-ligand interactions and by horizontal transfer of protein and nucleic acid cargo to the cells they engage.[30,31] There are two major classes of EVs, designated as microvesicles or large EVs (ranging from 250 nm to 1 micron in diameter)

which mature and bud off from the cell surface, and exosomes or small EVs (typically less than 200 nm in size) that form as intraluminal vesicles within multi-vesicular bodies (MVBs) and are released from cells upon the fusion of MVBs with the plasma membrane.[32,33] EVs have been extensively studied in cancer and shown to play important roles in shaping the TME and transforming stromal cells, as well as in their ability to induce angiogenesis, establish a pre-metastatic niche, and even mediate immune evasion.[34–37] Indeed, EVs derived from both GBM and melanoma cells have been shown to locally and systemically suppress the activation of $CD8^+$ T cells in a PD-L1-dependent manner.[38,39] Interestingly, several reports using different cancer cell types, including GBM, have implicated hyperactive PI3K and/or PTEN loss with the increased expression of PD-L1.[40–44] Therefore, we were interested in investigating how PTEN/PI3K signaling influences the biogenesis of EVs and the presence of PD-L1 as EV-associated cargo.

Using four isogenic glioma cell lines, we demonstrate that following IFN-γ treatment, cells lacking PTEN have a marked increase in both surface levels of PD-L1 and as EV associated cargo. We further show that upon PTEN depletion, cells exhibit an increase in total EV biogenesis. Both restoration of PTEN and pharmacological inhibition of PI3K reversed these observations, indicating that EV biogenesis and PD-L1 cargo sorting is regulated in a PI3K-dependent manner. Using a $Jurkat^{PD-1}$ reporter cell line, we show that EVs shed from glioma cells are capable of inhibiting TCR signaling in a dose-dependent manner with this effect being most pronounced when vesicles are shed from cells that lack PTEN.

Results

PTEN impacts cell surface levels of PD-L1 but not global protein levels

PTEN loss in GBM has been associated with the increased expression of PD-L1 in steady-state conditions.[40] However, given the recent appreciation that IFN-γ has a role in upregulating PD-L1 and in treatment outcomes relating to ICI, we re-examined the relationship between PTEN status and PD-L1 expression by using four glioma cell lines with previously confirmed PTEN status.[40,45] Using CRISPR technology, we knocked out *PTEN* in LN229 and T98G cells, and induced the ectopic expression of PTEN in U251 and U87 cells. First, we examined U251 and U87 cells to compare PD-L1 expression with or without IFN-γ treatment. Twenty-four hours post-treatment, cells were lysed and subjected to immunoblot analysis. As expected, PTEN expression reduced PI3K activity as indicated by decreased levels of phosphorylated AKT (p-AKT) (Figure 1A). Additionally, although there was a clear and marked upregulation of PD-L1 expression in response to IFN-γ treatment, there was no clear indication that PTEN/PI3K signaling impacted overall PD-L1 levels regardless of IFN-γ treatment (Figure 1A). To determine whether the same was true at the transcriptional level, we performed qPCR analysis on isogenic U87 and U251 cells with or without IFN-γ. IFN-γ treatment gave rise to the expected increase in PD-L1 transcripts; however, no difference in PD-L1 transcripts was observed in a PTEN-dependent manner either in the presence or absence of IFN-γ treatment (Figure S1A). We then broadened the comparison of PD-L1 expression across all four isogenic cell lines in response to IFN-γ. Apart from the T98G cell line, immunoblot data revealed that the manipulation of PTEN corresponded with the expected changes in the phosphorylation status of AKT, whereas the *PTEN* KO in LN229 cells led to increased p-AKT, the ectopic expression of PTEN

in U87 and U251 cells resulted in reduced p-AKT levels (Figure 1B). T98G cells harbor a point mutation in PTEN (L42R), resulting in impaired PTEN function and explains why *PTEN* KO had no impact on PI3K/AKT activity.[45] Importantly, across all cell lines, there was no clear indication that PTEN/PI3K signaling affected PD-L1 expression in response to IFN-γ (Figure 1B). Because IFN-γ can be present acutely or chronically within the context of a tumor, we wondered if temporal differences in IFN-γ exposure would lead to divergent PD-L1 expression patterns in a PTEN-dependent manner. However, no obvious differences in PD-L1 expression were observed between PTEN expressing and non-expressing U87 cells (Figure S1B). Taken together, these data suggested that the upregulation of PD-L1 in response to IFN-γ was occurring in a PTEN-independent manner.

It is known that IFN-γ binds to its cognate receptor to stimulate the JAK/STAT class of transcription factors to upregulate PD-L1 expression.[46] Therefore, we concomitantly treated U87 cells with IFN-γ, tofacitinib (a JAK/STAT inhibitor), or LY294002 (a PI3K inhibitor) to determine which signaling pathway could inhibit PD-L1 expression. Using immunoblot analysis, we again determined that reduced PI3K activity failed to inhibit PD-L1 expression regardless of IFN-γ treatment (Figure S1C). In contrast, tofacitinib successfully blocked IFN-γ mediated expression of PD-L1 in a dose-dependent manner (Figure S1D). Collectively, these data suggested that PD-L1 expression was independent of PI3K/AKT signaling and that IFN-γ mediated PD-L1 expression is dependent upon JAK/STAT signaling.

To determine whether any changes were exclusively happening at the cell surface, three isogenic cell lines for PTEN expression, LN229, U87 and U251 cells were analyzed by flow cytometry 24 hours after IFN-γ or PBS treatment. All cells treated with IFN-γ showed an increase in cell surface

PD-L1 expression; however, cells expressing PTEN had markedly reduced levels of PD-L1 at the plasma membrane (Figure 1C). The fact that PTEN appears to influence the extent to which PD-L1 is present at the cell surface raised the possibility that PTEN may be playing a role in the endocytic trafficking or regulation of cargo directed toward the PM. Indeed, it is beginning to be appreciated that PTEN can regulate endosomal maturation to influence and regulate mitotic signaling.[47] Because EVs originate from either the PM or endomembrane compartments, this led us to investigate whether the loss of *PTEN* and/or reduced PI3K signaling could influence EV biogenesis and the inclusion of PD-L1 as cargo.

A

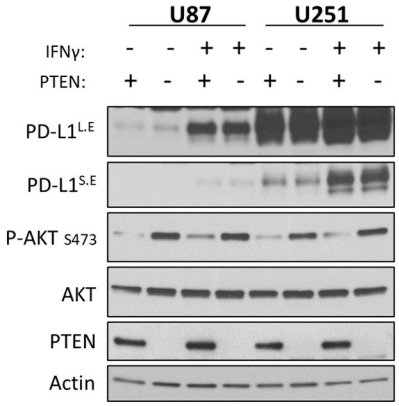
U87
U251
IFNγ: - - + + - - + +
PTEN: + - + - + - + -
PD-L1L.E
PD-L1S.E
P-AKT S473
AKT
PTEN
Actin

B

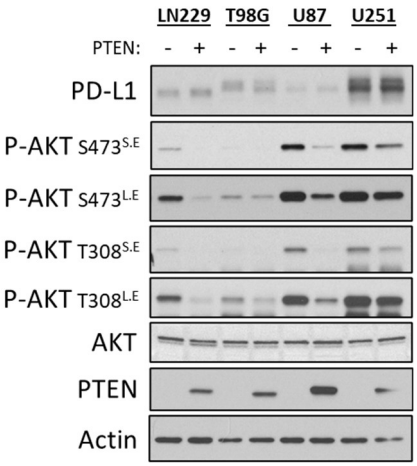
LN229
T98G
U87
U251
PTEN: - + - + - + - +
PD-L1
P-AKT S473S.E
P-AKT S473L.E
P-AKT T308S.E
P-AKT T308L.E
AKT
PTEN
Actin

C

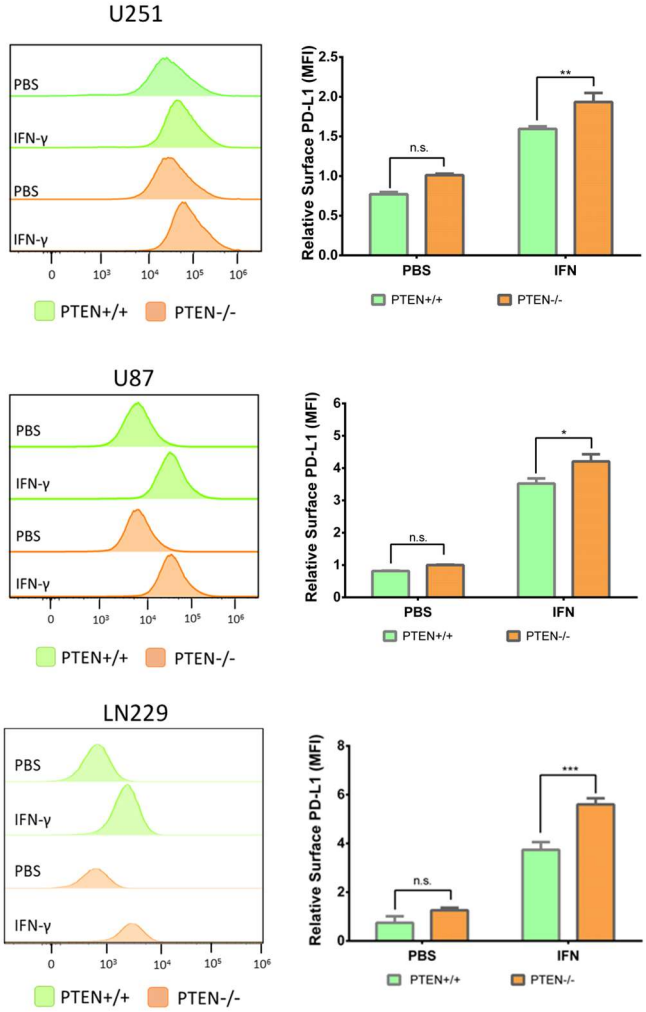
U251
PBS
IFN-γ
PBS
IFN-γ
0
10³
10⁴
10⁵
10⁶
PTEN+/+
PTEN-/-
Relative Surface PD-L1 (MFI)
2.5
2.0
1.5
1.0
0.5
0.0
n.s.
**
PBS
IFN
PTEN+/+
PTEN-/-
U87
PBS
IFN-γ
PBS
IFN-γ
PTEN+/+
PTEN-/-
Relative Surface PD-L1 (MFI)
6
5
4
3
2
1
0
n.s.
*
PBS
IFN
PTEN+/+
PTEN-/-
LN229
PBS
IFN-γ
PBS
IFN-γ
PTEN+/+
PTEN-/-
Relative Surface PD-L1 (MFI)
8
6
4
2
0
n.s.
***
PBS
IFN
PTEN+/+
PTEN-/-

Figure 1. PTEN loss leads to increased cell surface levels of PD-L1 after IFN-γ

A.) Semi-stable U251 and U87 cells transduced with empty vector control or with PTEN vector, were treated once with IFN-γ (50 ng/mL) or with PBS as a control. 24 hours later, cells were lysed and analyzed by immunoblot to compare PD-L1 expression, PTEN, total AKT, p-AKT (S473), and Actin was used as a loading control. **B.)** Semi-stable isogenic glioma cell lines were created by either CRISPR-mediated PTEN KO (LN229 and T98G cells) or by the ectopic expression of PTEN (U87 and U251 cells). Both naïve and modified PTEN groups were treated once with IFN-γ (50 ng/mL) or PBS as vehicle control. After 24 hours, cells were serum starved for 12-15 hours, lysed and subjected to immunoblot analysis to compare the relative expression of PD-L1, PTEN, AKT activation (T308, S473) and Actin were used as a loading control. "L.E" denotes long exposure while "S.E" denotes short exposure. **C.)** Semi-stable isogenic cell lines for PTEN expression, U251, U87 and LN229 were treated with IFN-γ (50 ng/mL) or PBS control for 24 hrs. Cells were dissociated, centrifuged and resuspended in ice cold FACS buffer supplemented with αPD-L1-PE antibody (1:100 v/v) on ice for 30 min. Cells were spun down and resuspended in FACS buffer and analyzed by flow cytometry to evaluate cell surface PD-L1 distribution. Left, representative histograms of PD-L1 expression represented by fluorescence intensity on the X-axis and the number of events (cells) on the Y-axis. Right, the mean fluorescence intensity (MFI) of 3 different experiments were averaged and analyzed for statistical significance. Data for LN229 cells were acquired from four clones, two with and two without PTEN expression and averaged. Statistical analysis for all graphs was done using 2-way ANOVA with Tukey multiple comparisons test. *p-value 0.0190, **p-value 0.0097, *** p-value 0.001

PI3K inhibition and PTEN expression negatively impacts extracellular vesicle biogenesis

We first examined whether PI3K/PTEN signaling and/or IFN-γ could impact EV biogenesis. Using the isogenic U87 cell line for PTEN expression and a pharmacological PI3K inhibitor (LY294002), we confirmed through Western blotting that both PTEN expression and LY294002 led to a corresponding decrease in p-AKT, and IFN-γ treatment led to the upregulation of PD-L1 expression (Figure 2A). To determine if these signaling patterns altered EV biogenesis, the conditioned media from these cells was processed using a differential centrifugation method (Figure S2A) to generate partially clarified media (PCM) which was subjected to nanoparticle tracking analysis (NTA) to determine whether the overall diameter and/or relative abundance of EVs changed in response to these treatment conditions. NTA revealed a 50% reduction in EV biogenesis in response to PI3K inhibition from both pharmacological and genetic approaches (Figure 2B), whereas IFN-γ treatment did not have a significant effect on the numbers of EVs shed from U87 cells regardless of their PTEN status (Figure 2B).

We next examined the effects of knocking out *PTEN* in LN229 cells. LN229 cells were subjected to CRISPR-mediated PTEN KO, and the selected clones showed significant increases in p-AKT (Figure 2C) as well as a 40% increase in the number of EVs shed from the cells (Figure 2D). Comparable results were observed when we transiently knocked down (KD) PTEN in LN229 cells (Figures S2B-D). Together, these data imply that the regulation of PI3K by PTEN is likely the predominant cause of reduced EV biogenesis.

A

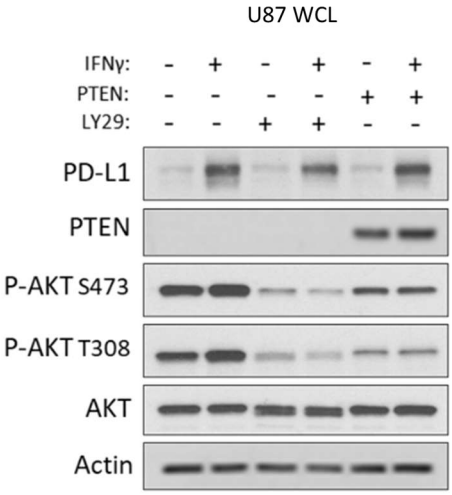
U87 WCL
IFNγ: - + - + - +
PTEN: - - - - + +
LY29: - - + + - -
PD-L1
PTEN
P-AKT S473
P-AKT T308
AKT
Actin

B

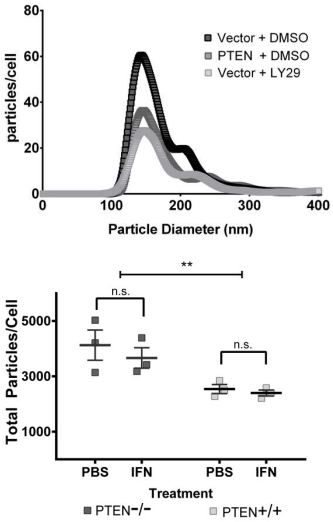
Vector + DMSO
PTEN + DMSO
Vector + LY29
particles/cell
Particle Diameter (nm)
**
n.s.
n.s.
Total Particles/Cell
PBS
IFN
PBS
IFN
Treatment
PTEN-/-
PTEN+/+

C

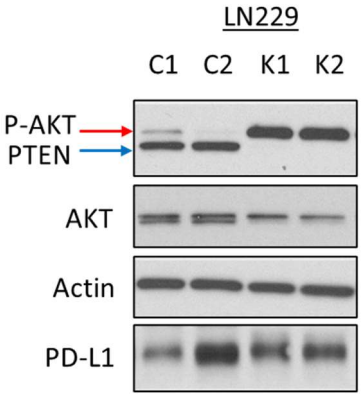
LN229
C1 C2 K1 K2
P-AKT
PTEN
AKT
Actin
PD-L1

D

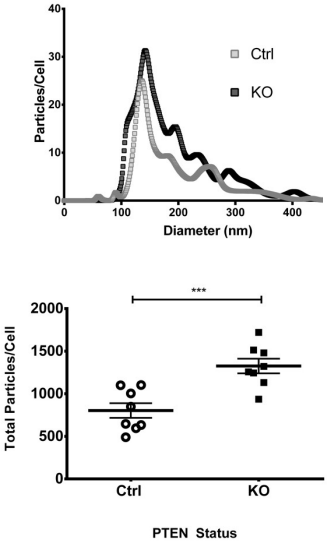
Ctrl
KO
Particles/Cell
Diameter (nm)
***
Total Particles/Cell
Ctrl
KO
PTEN Status

Figure 2. Elevated PI3K signaling is associated with increased EV biogenesis in LN229 and U87 cells

A.) Semi-stable U87 cells were concomitantly treated with the PI3K inhibitor, LY294002 (LY29, 30 µg/mL) or with DMSO as vehicle control and with IFN-γ (50 ng/mL) or PBS as control. 24 hours post-treatment, cells were washed three times and cultured for 12-15 hours in serum-free base media. The conditioned media was collected for downstream analysis. Cells were lysed and analyzed by immunoblot to compare PTEN, total AKT, active AKT (T308, S473) and Actin as loading control. B.) Conditioned media collected from treated U87 cells was processed by differential centrifugation to generate partially clarified medium (PCM) which contains all EV subtypes and analyzed by nanoparticle tracking analysis (NTA). Top, a representative NTA plot of U87 derived EVs measuring their diameter and abundance relative to cell number. Bottom, the total area under the curve from three different NTA experiments was used to calculate total EVs shed per cell. Two-way ANOVA using Tukey's multiple comparisons test, ** p-value .0032. C.) In a similar manner, two unique LN229 clones with confirmed CRISPR-mediated KO of PTEN (K1, and K2) and two control scramble CRISPR treated LN229 clones (C1, and C2) were used to compare PI3K signaling and EV production. As before, cells were cultured in full serum media and washed three times with base media or PBS and then cultured in serum-free media for 12-15 hours. Cells were lysed and analyzed by immunoblot to compare, PTEN, total AKT, active AKT (T308, S473), and Actin as the loading control. D.) NTA was performed on the PCM of these cells from four different experiments to evaluate total EVs produced per cell. Two-way ANOVA using Tukey's multiple comparisons test, *** p-value 0.0007.

PTEN/PI3K signaling regulates PD-L1 and other EV associated cargo

Earlier, we showed that the treatment of U87, U251, and LN229 cells with IFN-γ led to an increase in PD-L1 localized at the cell surface. However, when these cells lacked PTEN, the levels of PD-L1 were markedly elevated over their PTEN expressing counterparts (Figure 1C). We then examined whether this would result in elevated levels of PD-L1 in EVs. U87 cells with or without PTEN were treated with IFN-γ or PBS as control for 24 hours. The cells were washed with serum-free media and cultured for 12-15 hours. The conditioned media was then collected and processed to generate PCM. To determine whether any changes in EV cargo were specific to a distinct subtype of EVs, the PCM for each condition was subjected to centrifugation at 15,000 x g to obtain large EVs (microvesicles) or what is referred to as the "P15" fraction. The resulting supernatant was subjected to a subsequent ultracentrifugation step of 120,000 x g to obtain the small EVs (exosomes) or the "P120" fraction (Figure S2A). Immunoblot analysis was performed on both whole cells and their respective P15 and P120 EV fractions to compare protein cargo. As was previously observed, U87 cells exhibited an upregulation in PD-L1 expression in response to IFN-γ treatment in a PTEN-independent manner (Figure 3A). Because we had previously observed a significant reduction in EV biogenesis when PI3K signaling was inhibited, we analyzed equal protein content for each EV subtype. When cells lacked PTEN expression, IFN-γ treatment led to a considerable enrichment of PD-L1 in both EV subtypes (Figure 3B). Surprisingly, however, in cells expressing PTEN, the amount of PD-L1 was markedly reduced, predominantly within the P120 exosome fraction (Figure 3B). To establish whether these effects were specific to PD-L1, we probed for other proteins that were reported to be included in the cargo of U87-derived EVs such as the EGFR[48] and Ras[49]. In fact, both signaling proteins exhibited a similar PTEN-dependent

reduction in their presence within the P120 EV fraction (Figure 3B). No changes in CD81 and Flotillin-II were observed, suggesting that some specificity of cargo sorting existed.

To establish whether these changes were occurring in a PI3K-dependent manner, we repeated these experiments using a PI3K inhibitor (LY294002). Immunoblot analysis confirmed that cells treated with LY294002 had significantly reduced p-AKT activity and IFN-γ treatment leading to an increase in PD-L1 expression (Figure S3A). Indeed, as we had previously observed upon ectopic expression of PTEN, cells treated with LY294002 produced EVs with reduced quantities of PD-L1, EGFR, and Ras within the P120 EV fraction while leaving Flotillin-II and CD81 unaffected (Figure S3B). These results indicate that the PTEN-mediated inhibition of PD-L1 and other cargo are occurring in a PI3K-dependent manner in U87 cells.

To determine whether these results extended beyond U87 cells, we examined the effects of PTEN expression in U251 cells and LN229 cells. As previously observed, U251 cells ectopically expressing PTEN showed reduced p-AKT while leaving PD-L1 expression unchanged (Figure 3C). Immunoblot analysis confirmed that PTEN expression in U251 cells also led to a marked reduction in PD-L1 and Ras cargo in the P120 EV fraction (Figure 3D). Similarly, CRISPR-mediated PTEN KO in LN229 cells also resulted in elevated p-AKT (Figure 3E) and a corresponding enrichment of PD-L1 and EGFR in their derived EVs (Figure 3F). Collectively, these data suggest that PTEN loss leads to the enrichment of PD-L1 and other cargo within the P120 EV fraction shed by cells in a PI3K-dependent manner. Indeed, when we expressed the constitutively active form of the EGFR (EGFRvIII) in U87 cells, which results in hyperactive PI3K/AKT activation (Figure S3C), an increase in PD-L1 associated with the P120 EV fraction (Figure S3D) and in EV biogenesis (Figure S3E) was observed. The fact

that these results were observed across multiple cell lines using different methods suggests that a conserved PTEN/PI3K dependent process broadly regulates EV biogenesis and the loading of their associated cargo. Importantly, because the loss of PTEN leads to an increase in the numbers of EVs produced and an enrichment in the PD-L1 cargo associated with the vesicles, we hypothesized that these cells would inhibit TCR signaling relative to their PTEN expressing counterparts.

A

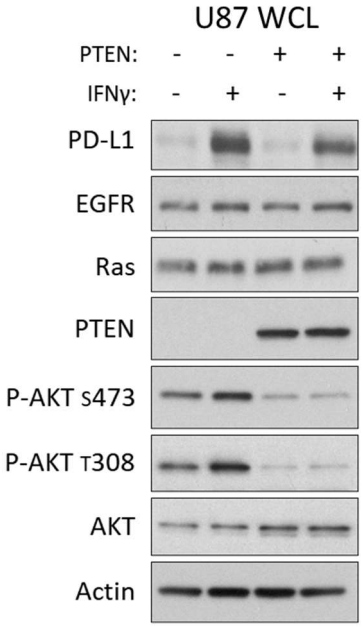
U87 WCL
PTEN: - - + +
IFNγ: - + - +
PD-L1
EGFR
Ras
PTEN
P-AKT S473
P-AKT T308
AKT
Actin

B

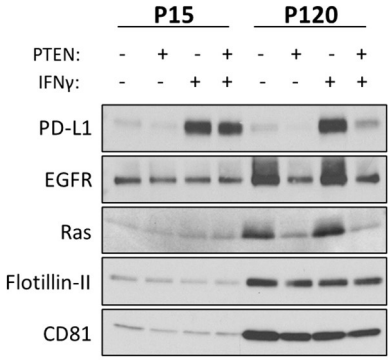
P15
P120
PTEN: - + - + - + - +
IFNγ: - - + + - - + +
PD-L1
EGFR
Ras
Flotillin-II
CD81

C

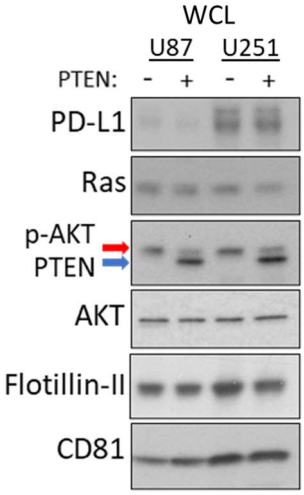
WCL
U87
U251
PTEN: - + - +
PD-L1
Ras
p-AKT
PTEN
AKT
Flotillin-II
CD81

D

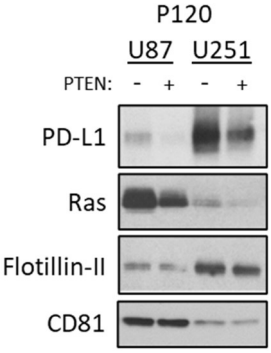
P120
U87
U251
PTEN: - + - +
PD-L1
Ras
Flotillin-II
CD81

E

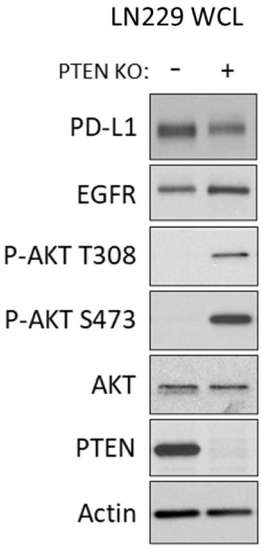
LN229 WCL
PTEN KO: - +
PD-L1
EGFR
P-AKT T308
P-AKT S473
AKT
PTEN
Actin

F

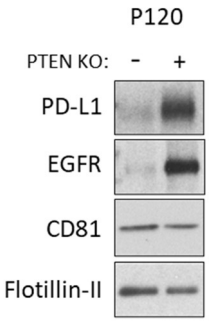
P120
PTEN KO: - +
PD-L1
EGFR
CD81
Flotillin-II

Figure 3. PTEN/PI3K signaling impacts protein sorting of PD-L1 in glioma derived EVs

A.) Semi-stable U87 cells, with or without PTEN, were treated with IFN-γ (50 ng/mL) or PBS as the vehicle control. 24 hours later, cells were washed three times and cultured in serum free media for 12-15 hours. Whole cell lysates (WCL) were prepared and subjected to immunoblot analysis to evaluate expression of PTEN, AKT, AKT activity (T308, S473), Actin as a loading control, and EV associated cargo of interest, including PD-L1, EGFR, and Ras **B.)** The PCM of each treatment group was subjected to a 15,000 x g spin for 1 hour to collect the P15 or microvesicle fraction. The remaining media was centrifuged for 4 hours at 120,000 x g to collect the P120 or exosome fraction. Within each EV subtype, equal protein was loaded but between EV subtypes each is represented by their relative abundance. Cargo of interest, including PD-L1, EGFR, and Ras were used to compare cargo changes relative to the WCL. CD81 was used as a marker to identify the enrichment of exosomes (P120) while Flotillin-II was used as a loading control. **C.)** In a similar fashion, immunoblot analysis was used to compare whether PTEN expression could impact U251 derived P120 cargo. U87 cells were also analyzed in parallel to compare relative differences. As before, immunoblot analysis was carried out on WCL of cells to evaluate PTEN expression, p-AKT levels and EV related cargo of interest including PD-L1, Ras, Flotillin-II, and CD81. **D.)** The P120 EV fraction from these cells was collected as before, lysed, and analyzed by immunoblot analysis. Each condition had equal protein loaded to evaluate whether PTEN expression could alter PD-L1, Ras, and common EV markers including Flotillin-II, and CD81. **E.)** To evaluate if PTEN deletion could elicit the reciprocal results, CRISPR mediated PTEN KO (K1) or CRISPR control (C1) LN229 cells were treated with IFN-γ (50 ng/mL) for 24 hours and prepared as before for EV collection. Immunoblot analysis of whole cells was performed for PD-L1, EGFR, PTEN, AKT, p-AKT (S473, T308) and Actin as the loading control. **F.)** P120 EV fraction was collected as before and subjected to immunoblot analysis to compare PD-L1, EGFR, CD81 and Flotillin-II. All lysates were equally loaded for protein concentration.

EVs shed from PTEN-null cells have an increased capability to inhibit TCR signaling

In $CD8^+$ T cells, the activation of PD-1 by PD-L1 has been shown to recruit phosphatases that attenuate TCR signaling which ultimately impairs T cell function.[50] Importantly, *in vivo* models have shown that EV-associated PD-L1 is capable of suppressing cytotoxic $CD8^+$ T cell function both locally and systemically.[38,39] Because we observed both greater numbers of EVs shed and enriched levels of PD-L1 associated in EVs from cells lacking PTEN, we examined whether these cells would be able to suppress TCR signaling to a greater extent than their PTEN expressing counterparts. To answer this question, we turned to the Jurkat lymphoma cell line as a well-established model system for studying TCR signaling.[51] In order to quantify TCR activity, we used a luciferase Jurkat reporter cell line that is driven by nuclear factor of activated T-cells (NFAT). TCR-mediated activation of NFAT allows for the transcription of several T cell effector cytokines such as IL-2, IL-4, IL-10, and IFN-γ and thus functions as a reliable proxy for TCR activity.[52] Importantly, because Jurkat cells do not endogenously express the PD-1 receptor, we transduced the reporter Jurkat cells with PD-1 and used fluorescent activated cell sorting (FACS) to retain the highest expressors of PD-1, hereafter referred to as $Jurkat^{PD-1}$ cells (Figure S4A and S4B). Finally, the function of the luciferase reporter system in the $Jurkat^{PD-1}$ cells was confirmed by using a stimulating αCD3 (OKT3) antibody with endpoints at 3-, 6-, and 20-hours post-treatment (Figure S4C). From these data, we calculated the EC50 for αCD3 to be 50 ng/mL which was used alongside the 6-hour time point for the remainder of our experiments.

We then examined whether glioma derived EVs were capable of inhibiting $Jurkat^{PD-1}$ TCR activity by first utilizing the U251 cell line due to its robust expression of PD-L1 within their EVs relative to

U87 cells (Figure 3D). To confirm whether any observed TCR inhibition was occurring in a PD-1/PD-L1 specific manner, Jurkat^{PD-1} cells were either pre-treated with an inhibitory αPD-1 antibody, or an isotype control antibody 30 minutes prior to the simultaneous treatment with the stimulating αCD3 antibody and three different doses of EVs. Six hours post-treatment, cells were treated with luciferase substrate and luminosity readings were taken. Indeed, we observed a dose-dependent reduction in luminosity (TCR activity) that could be rescued by the pre-treatment of Jurkat^{PD-1} cells with an inhibitory αPD-1 antibody (Figure 4A), indicating that these effects were specific to EV associated PD-L1.

We then examined whether the IFN-γ mediated upregulation of PD-L1 would influence the magnitude of EV-mediated TCR inhibition, and whether this changed in response to PTEN status. To help us determine the extent of PD-1/PD-L1 specific TCR signal attenuation, we used Jurkat^{PD-1} and PD-1 naïve Jurkat^{Ctrl} cells. Jurkat cells were treated with a moderate (++) dose of EVs shed from either PTEN expressing or non-expressing U87 cells with or without IFN-γ. Overall, EVs derived from U87 cells treated with IFN-γ had a greater capability of inhibiting TCR signaling relative to the EVs shed from PBS treated cells (Figure 4B). More specifically, EVs from U87 cells expressing PTEN and treated with IFN-γ were only able to limit TCR signaling by 20%, compared to the 10% inhibition observed for EVs shed from the PBS treated control group. In contrast, EVs from parental U87 cells (PTEN-null) treated with IFN-γ led to a 50% reduction in TCR signaling, whereas EVs from the same cells without IFN-γ treatment, only resulted in 15% signal attenuation. Thus, PTEN expression significantly and negatively impacted EV-mediated TCR inhibition, essentially eliminating any benefits conferred by IFN-γ treatment. To further illustrate that these inhibitory effects were specific to PD-1/PD-L1 function, EVs from IFN-γ treated U87 cells, with or without PTEN expression, were used to treat Jurkat^{PD-1} cells that were either pre-treated with an inhibitory αPD-1 antibody or an isotype control antibody. As we had previously observed, EVs from U87 cells lacking PTEN expression were significantly better at inhibiting TCR signaling; however, these effects were essentially reversed when Jurkat^{PD-1} cells were pre-treated with the αPD-1 antibody (Figure 4C). Taken together, these data indicate that EVs can indeed suppress TCR signaling in a dose-dependent and PD-L1-specific manner. Most importantly, these data show that glioma cell lines lacking PTEN expression are likely better suited to evade immune detection in response to

IFN-γ and implicate EVs as potentially important contributors in the formation of adaptive immune resistance.

A

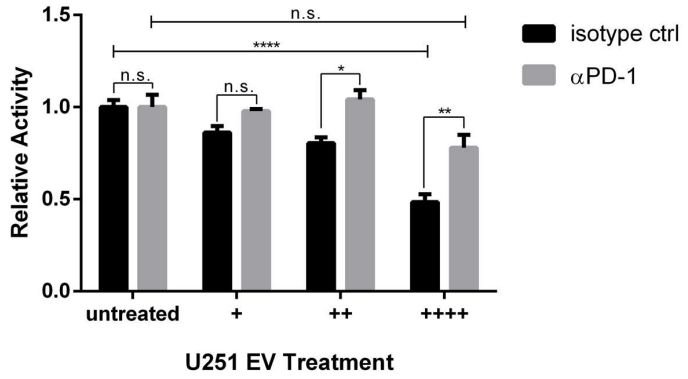
1.5
1.0
0.5
0.0
Relative Activity
n.s.
****
n.s.
n.s.
*
**
untreated
+
++
++++
U251 EV Treatment
isotype ctrl
αPD-1

B

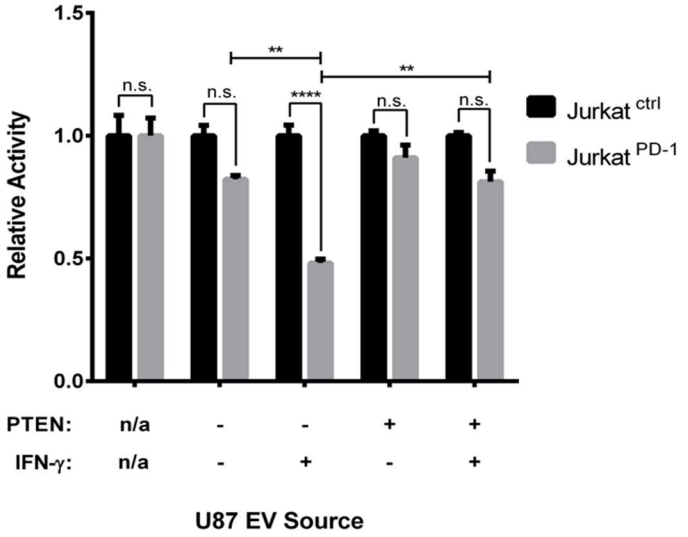
1.5
1.0
0.5
0.0
Relative Activity
**
**
n.s.
n.s.
****
n.s.
n.s.
PTEN: n/a - - + +
IFN-γ: n/a - + - +
U87 EV Source
Jurkat ctrl
Jurkat PD-1

C

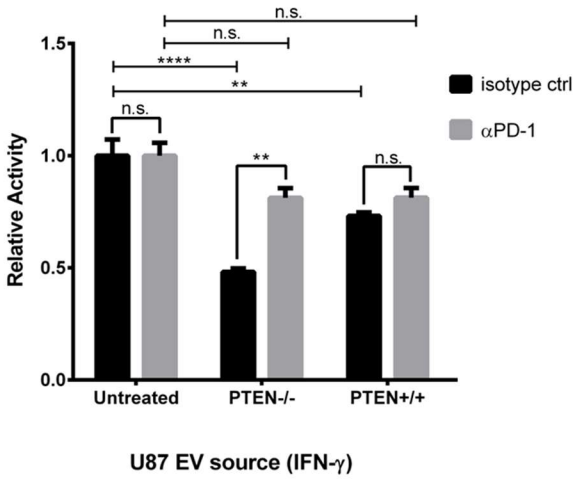
1.5
1.0
0.5
0.0
Relative Activity
n.s.
n.s.
****
**
n.s.
**
n.s.
Untreated
PTEN-/-
PTEN+/+
U87 EV source (IFN-γ)
isotype ctrl
αPD-1

Figure 4. EVs from glioma cell lines abrogate TCR signaling in a dose dependent and PD-L1/PD-1 specific manner

U251 cells overexpress PD-L1 even in the absence of IFN-γ stimulation. For this reason, we used these cells to establish a baseline for any EV/PD-L1 mediated inhibition. **A)** Jurkat^{PD-1} cells were concomitantly treated with one of three EV doses and with activating αCD3 (OKT3) antibody at 50 ng/mL. A separate group of Jurkat^{PD-1} cells were pre-treated with either an inhibitory αPD-1 or isotype control antibody 30 min before EV treatment. An EV treatment of (++++) corresponds to about 4.2 x 10^8 particles and was used to treat one well of 3 x 10^4 Jurkat^{PD-1} cells with (++) and (+) EV doses being halved relative to original dose. Luciferase values were normalized to isotype control Jurkat^{PD-1} cells for each condition. As a result, the Y-axis represents relative luciferase units (RLU). p-values: * 0.0398, **0.0035 **** < 0.0001 **B)** Jurkat^{PD-1} and Jurkat^{Ctrl} cells were simultaneously treated with OKT3 αCD3 antibody (50 ng/ml) and total EVs derived from U87 cells with or without PTEN expression and with or without IFN-γ (50 ng/ml). EV dose was sourced from 1.25 x 10^6 U87 cells, about 3.2 x 10^9 particles from PTEN positive cells or 5 x 10^9 particles from parental PTEN naïve U87 cells and used to treat 3 x 10^4 Jurkat^{PD-1} cells. Jurkat^{Ctrl} cells within each treatment condition were used to normalize luciferase activity. **C)** To determine if EV mediated inhibition was specific to PD-L1, Jurkat^{PD-1} cells were pre-treated with αPD-1 antibody or isotype control antibody for 30 min before introducing the same EV treatment as above. Luciferase values were normalized to isotype treated Jurkat^{PD-1} cells for each treatment condition. Each experiment was done in triplicate and repeated twice. Statistical analysis was done by two-way ANOVA with Tukey multiple comparison. p-value **** < 0.0001, ** < 0.0080

Discussion

It is becoming increasingly clear that intrinsic molecular and genomic characteristics of GBM have important immuno-regulatory functions.[22,47] In particular, the loss of PTEN has garnered increased clinical significance due to its prevalence in GBM patients, and its ability to shape tumor-immune relationships important for disease progression and immune evasion.[48,49] Cancer cells can escape immune detection by adaptively upregulating PD-L1 in response to extrinsic factors such as IFN-γ,[50,51] and/or because of oncogenic PI3K/AKT activity.[40–44] Whether these two signaling pathways influence one another in GBM, however, has not been clear. Here, we have used several isogenic cell lines and pharmacological inhibitors to investigate how these two signaling pathways independently and/or synergistically impact PD-L1 expression. We found that in glioma cell lines, PTEN status had no impact on overall PD-L1 expression at the protein or transcriptional level. While our qPCR data agrees with another GBM study by Parsa and colleagues, our immunoblot data does not support their theory of increased translation of PD-L1 transcripts as a result of hyperactive PI3K/AKT[40]. The differences in our results are likely explained by different culture conditions as we conducted our experiments in the absence of serum which can negatively impact mTORC1 activity and translational machinery.[52] We then examined whether IFN-γ would influence these results and found that it promoted elevated levels of PD-L1 expression at the protein and transcriptional level. We observed that this occurs in a JAK/STAT-dependent manner and independent of PTEN expression and PI3K signaling. Similar observations have been reported in colorectal and NSCLC cancer models.[42,44] Importantly, flow cytometry revealed that PTEN expression negatively impacts PM-associated PD-L1 levels only after IFN-γ treatment. Because EVs

either mature and bud off from the cell surface (i.e., MVs) or are shed as a result of the fusion of MVBs with the plasma membrane (exosomes), and since various lines of evidence have highlighted their role in PD-L1 mediated immune evasion, we suspected that our results were indicative of underlying changes in EV associated PD-L1 cargo and biogenesis. However, no study to date has evaluated whether PTEN/PI3K and IFN-γ signaling influence EV biogenesis and PD-L1 cargo.

We now present evidence that links the loss of PTEN to enhanced EV biogenesis. These results were confirmed both by the ectopic expression of PTEN or its KO in U87 and LN229 cells, respectively. We also examined whether IFN-γ could alter EV biogenesis and whether its ability to upregulate PD-L1 in different EV subtypes might be affected by PTEN expression. Interestingly, although we did not observe any significant changes in EV biogenesis in response to IFN-γ treatment (regardless of PTEN status), it did result in an enrichment in PD-L1 in both the larger P15 EVs (microvesicles) and smaller P120 EVs (exosomes) isolated from cells lacking *PTEN*. Strikingly, cells expressing PTEN had significantly reduced levels PD-L1 in their P120 EV fraction. As a result, then, it can be said that PTEN loss leads to a considerable increase in the bioavailability of PD-L1 in the extracellular milieu of cells. We then developed a Jurkat^{PD-1} NFAT reporter cell line to measure TCR signaling and found that EVs shed and isolated from glioma cells are capable of inhibiting TCR signaling in a dose-dependent and PD-L1-specific manner. Most importantly, cells treated with IFN-γ produced EVs with an enhanced capacity to inhibit TCR signaling only when they lacked PTEN expression. Therefore, IFN-γ induced adaptive immune resistance is likely impaired in cells expressing PTEN as a result of reduced EV biogenesis and PD-L1 associated cargo. Our results suggest that cancer cells lacking PTEN are better able to evade immune detection in

response to IFN-γ and highlight disruptions in EV biogenesis and cargo as important variables in shaping immune evasion.

Because our data reveals that PTEN expression can negatively regulate EV cargo, it raises the question as to what other cargo and immune cell types might be impacted. For example, studies have shown EVs can be enriched with FasL, TRAIL, and galectin-9, which promote T cell apoptosis, suppress TCR expression, and block cytotoxic functions of NK and $CD8^+$ T cells.[53–55] Additionally, because IFN-γ is known to induce other interferon response genes (IRGs) with varying immunomodulatory functions and clinical significance,[5] future studies will be required to obtain a full understanding of the role PTEN/PI3K and IFN-g have in shaping EV-mediated control of the TIME beyond just T cells.

Another important question concerns the molecular mechanism by which impaired PI3K signaling, as a result of PTEN expression or pharmacological inhibition, can lead to the enrichment of EV associated PD-L1 cargo and an increase in EV biogenesis. Because we did not observe any PTEN-dependent differences in total PD-L1 at the protein or mRNA level, perhaps the most plausible explanation for the enrichment of PD-L1 at the PM is the result of reduced endocytic behavior which subsequently alters exosome biogenesis and cargo sorting which originate within endosomal MVB compartments. Indeed, PTEN has been suggested to serve as a novel regulator of endocytic events as a result of both its lipid and protein phosphatase abilities.[56] However, given that PI3K inhibitors yield similar results as those obtained when PTEN levels are depleted, the activation of PI3K activity as an outcome of PTEN loss appears to be largely responsible of our findings. It has been shown that reduced levels of PI(4,5)P2, PTEN ablation, and PI3K inhibition can

all lead to impaired endocytosis, aberrant protein recycling, and the accumulation of PM-associated proteins.[57–59] Indeed, because PIP metabolism is subject to tight spatial/temporal regulation, wherein one PIP will act as a precursor for a lipid kinase or phosphatase, [60] disruptions in a single lipid kinase or phosphatase can thus impact organelle identity, protein recruitment, endocytosis, endocytic trafficking, autophagy, cytoskeletal rearrangement and the regulation of cellular signaling events.[61,62] For example, a recent biochemical study of PTEN has found that its capacity to negatively regulate PI3K/AKT is dependent on its ability to localize onto PI(3)P enriched endosomes through its C2 domain. [63] Thus, the possibility that PTEN loss or hyperactive PI3K, could impact exosome biogenesis and cargo sorting as a result of altered PIP dynamics is an attractive theory to consider. In fact, the disruption of VPS34 (*PIK3C3)* activity, the sole lipid kinase to generate PI(3)P, was shown to lead to the release of atypical exosomes in the context of neurodegenerative disease.[64] Similarly, the inhibition of the PIKfyve lipid kinase, which generates the endosome and MVB-specific PI(3,5)P2 from PI(3)P, has also been reported to give rise to increased exosome biogenesis.[65] Therefore, future studies will be directed toward further elucidating the biochemical mechanisms by PI3K and altered PIP metabolism in discrete membrane compartments can impact endomembrane trafficking and the recruitment of specific cargo into EVs.

Methods

Cells

U87MG, LN229, U251, and T98G cells were obtained from American Type Cell Culture (ATCC). Jurkat cells expressing the NFAT luciferase reporter were purchased from Promega (#J1601). Apart from Jurkat cells, all cell lines were maintained in Dulbecco's Modified Eagle Medium (DMEM) supplemented with 10% fetal bovine serum (FBS). Jurkat cells were maintained in Roswell Park Memorial Institute 1640 (RPMI, Thermo #118750) medium supplemented with 10% fetal bovine serum (FBS, Thermo #16000044), 1 mM sodium pyruvate (Thermo #11360070) and 100 nM minimal non-essential amino acids (Thermo #11140050). Transduced semi-stable cells were cultured in their respective media supplemented with 250 ng/mL puromycin. Adherent cells were subcultured by washing once with 1x phosphate buffered saline (PBS) and dissociated by incubating cells with Hank's balanced salt solution (HBSS) containing 0.25% Trypsin, 0.1% EDTA w/o Calcium, Magnesium and Sodium Bicarbonate (Corning #25053) for 3 minutes at 37°C. Complete media was used to quench trypsin's activity followed by centrifugating cells at 200 x g for 5 minutes. Jurkat cells were seeded at a density of 1×10^6 cells per mL of media and subcultured every 3 days by collecting and centrifugating floating cells at 400 x g for 5 minutes. In some instances, cells were treated with the JAK/STAT inhibitor Tofacitinib citrate (Cayman Chemical #11598), IFN-γ (Peprotech #300-02), or the PI3K inhibitor LY294002 (Cayman Chemical #70920) at the indicated time and concentrations mentioned.

RNA Isolation and Quantitative PCR Analysis

Total RNA from cells was isolated using Direct-zol RNA miniprep kits (Zymo Research, #R2051). RNA concentration was measured on a NanoDrop OneC (ThermoFisher) instrument. 500 ng of total RNA was converted to cDNA using Superscript III Reverse Transcriptase (Invitrogen) and oligo dT_{20} primers. The cDNA was then used to determine the expression levels of the indicated transcripts using SYBR Green Supermix (Bio-Rad) in an Applied Biosystems ViiA 7 Real-Time PCR System using the ΔΔCT method. The following primers were used for the RT-qPCR analyses: PD-1 (CD274) Forward: GCTGCACTAATTGTCTATTGGGA

PD-1 (CD274) Reverse: AATTCGCTTGTAGTCGGCACC

β-actin Forward: CATGTACGTTGCTATCCAGGC

β-actin Reverse: CTCCTTAATGTCACGCACGAT

DNA constructs, cloning, subcloning and sequencing

The pLJM1-empty (#91980), and PD-1-miSFIT-1x (#124679) vectors were purchased from Addgene. PTEN and PD-1 were subcloned into linearized pLJM1-empty vector using EcoR1 and NHE1 restriction enzymes (NEB) and Takara's two-step In-Fusion® snap assembly (#638948) according to the manufacturer's recommendations. *PD-1* was subcloned from the PD-1-miSFIT-1x construct using the forward primer: CGTCAGATCCGCTAGCCTGGAGACGCCATCCACG and reverse primer: TCGAGGTCGAGAATTCCGGAAGCTGCGCCTGTCATC. *PTEN* was cloned from cDNA generated from LN229 mRNA using forward (ATGACAGCCATCATCAAAGAGATCGTTA) and reverse (TCAGACTTTTGTAATTTGTGTATGCTGATCTTCATCAA) primers. The subcloned PTEN was then subjected to a second round of PCR using the forward primer

(CGTCAGATCCGCTAGCCCACCATGGATTACAAGGATGAC) and reverse (TCGAGGTCGAGAATTCTCAGACTTTTGTAATTTGTGTATGC). For all genes, the InFusion reaction mixture was used to transform Takara's Stellar™ competent cells (#636766) using the heat shock method. For constructs needing higher DNA yields, Invitrogen One Shot™ Stbl3™ Chemically Competent E. coli cells were used (#C737303). To generate PTEN KO cells, two previously validated PTEN pLentiCRISPRv2 gRNAs[66] were purchased through GenScript (ACCGCCAAATTTAATTGCAG and TTATCCAAACATTATTGCTA). Scramble lentiCRISPRv2 construct (Addgene, #169795) was used as a control sgRNA. Qiagen QIAprep Spin Miniprep Kit was used to isolate all plasmid DNA. DNA sequences were validated by Sanger sequencing at the Cornell Biotechnology Resource Center. All primers were purchased from Integrated DNA technologies (IDT)

For gene knockdown (KD) studies, MISSION® TRC shRNA Lentiviral Vectors (Sigma) were used. LN229 cells were treated with five different PTEN shRNA constructs:

TRCN0000002746: CCGGCCACAGCTAGAACTTATCAAACTCGAGTTTGATAAGTTCTAGCTGTGGTTTTT

TRCN0000002748: CCGGCGTGCAGATAATGACAAGGAACTCGAGTTCCTTGTCATTATCTGCACGTTTTT

TRCN0000002749: CCGGCCACAAATGAAGGGATATAAACTCGAGTTTATATCCCTTCATTTGTGGTTTTT

TRCN0000230369: CCGGTATACCATCTCCAGCTATTTACTCGAGTAAATAGCTGGAGATGGTATATTTTTG

TRCN0000230370: CCGGCCACAAATGAAGGGATATAAACTCGAGTTTATATCCCTTCATTTGTGGTTTTTG

Lentivirus production and transduction

HEK-293T cells were transfected using the FuGENE® 6 Transfection Reagent (Promega) using the manufacturer's recommendations. Briefly, 33 µl of FuGENE® 6 solution was added to 570 µl of Opti-MEM™ reduced serum medium and incubated for 5 min. 1 µg of the DR8.2 packaging

construct (Addgene #8455) and 5 µg of the PMD2.G envelope construct (Addgene # 12259) were added to the solution, followed by the addition of 5 µg of either pLJM1-Empty, pLJM1-PTEN, pLJM1-PD-1, PTEN pLentiCRISPRv2 or shRNA constructs, and allowed to incubate for an additional 15 min. The transfection mixture was then added dropwise to 5 x 10^6 293T cells in a 10 cm tissue culture treated plate. Supernatant was collected 24 and 48 hours after transfection. Each viral collection was subjected to centrifugation at 500 x g for 10 min and pooled together. Viral supernatant was used fresh when possible or frozen at -80°C until needed.

All cells were transduced with a 1:1 mixture of viral supernatant and complete media, containing Polybrene (8 µg/mL) and 1x pen/strep for 8-12 hours. Jurkat cells were transduced by spinfection. Briefly, a 1:1 mixture of viral supernatant and complete media were incubated with 6 x 10^6 cells for 30 minutes at 37°C followed by centrifugation at 300 x g for 30 minutes at 37°C. All cells were allowed to recover in complete media for at least 48 hours before antibiotic selection. Semi-stable cell lines were generated by selecting cells with puromycin (1-2 µg/mL) for 5 days, with media being replaced every 24 h. On the sixth day, cells were maintained at 250 ng/mL puromycin. Cells treated with shRNA lentivirus were not selected using puromycin. Instead, following the 48 h recovery period, cells were immediately used for their appropriate experiments such as EV collection and/or immunoblot analysis.

For genetic knockouts using CRISPR, LN229 and T98G cells lines were transduced as above with both PTEN pLentiCRISPRv2 gRNAs or with scramble lentiCRISPRv2 and treated exactly as stated above for adherent cells. After antibiotic selection, cells were sub-cultured at a density of 1.5 cells/well in a 96 well plate in the presence of 250 ng/ml puromycin to select for individual clones.

Media was replaced every 3-4 days for 2 weeks. At the end of week 2, marked wells with single colony growth were sub-cultured and expanded. KO of PTEN was confirmed by immunoblot analysis.

Extracellular vesicle collection

For immunoblot analysis, 1.5 x 10^6 semi-stable cells were seeded in three 15 cm tissue-culture treated plates (Corning) for each treatment condition used. The following day, cells were treated with IFN-γ (50 ng/ml) or PBS as control. After twenty-four hours, cells were washed three times with PBS or base media and cultured overnight for 12-15 hrs. For each treatment group, three dishes were counted using a Bio-Rad TC20 cell counter in order to normalize EVs shed by cells by NTA or comparing protein changes by immunoblot analysis. EVs were collected by differential centrifugation (Figure S2A). The conditioned media was centrifuged at 300 x g for 5 min, transferred to a new tube, and subjected to a second spin at 500 x g for 10 min. This partially clarified media (PCM) was then transferred into 70 ml Beckman polycarbonate bottles (#355655) and subjected to ultracentrifugation at 15,000 x g (P15) for 1 hr using a Beckman type 45ti rotor. The supernatant was carefully removed and transferred to a new set of 70 ml polycarbonate bottles and centrifuged at 120,000 x g for 4 hours (P120). The initial P15 pellet was then resuspended and washed in PBS and subjected to another spin in a Beckman TLA 100.4 rotor at 15,000 x g (19,000 RPM). The washed P15 pellet (microvesicles) was then resuspended in either RPMI for biological experiments or lysed for immunoblot analysis. The P120 pellet was also resuspended and washed in PBS and subsequently spun in a TLA 100.4 rotor at 120,000 x g (54,000 RPM). The P120 pellet (exosomes) was either lysed or resuspended in RPMI for intended

experimental analysis. In a similar manner, EVs for Jurkat experiments were produced by seeding 5 x 10^5 U87 or U251 cells in 10cm dishes. Total EVs were collected for these experiments by centrifuging PCM at 120,000 x g and washing the pellet in PBS. The resulting EV pellet was resuspended in RPMI and used as described below. All centrifugation steps were carried out in pre-chilled rotors at 4°C.

Nanoparticle tracking analysis

PCM was analyzed by nanoparticle tracking analysis on a Malvern Nanosight 3000 at the Cornell Nanofabrication Facility (CNF) with a The camera level set to 12 and a threshold value of 7. Video was captured five times for 60 seconds for each sample. The total number of cells used to source EVs was used to normalize particle (EV) counts. Cell numbers were acquired after collecting the conditioned media using the Trypsin subculturing technique described above.

Immunoblotting

One confluent 15cm dish of cells was lysed by using 1 mL of lysis buffer (25 mM Tris HCL pH 7.6, 100 mM NaCl, 1% Triton X-100, 1 mM DTT, 1 mM EDTA, 1 mM NaVO4, 1mM NaF, 1 mM β-glycerol phosphate, and 1 mg/mL each of aprotinin and leupeptin) followed by cell scraping to produce whole cell lysates (WCL). For EV lysates, 200 µL of lysis buffer (without DTT) was used to lyse total EVs, or the individual P15 and P120 pellets. Protein concentration was analyzed using Bradford reagent (Bio-Rad, #5000006) with absorbance measured at 595 nm on a Beckman UV spectrophotometer. Unless otherwise noted, all lysates were subjected to SDS-PAGE on 4-20% TrisGlycine gels (Invitrogen). WCL and EV lysates were prepared with reducing or non-reducing 5x sample buffer, respectively, followed by boiling samples for 5 min. Lysates were loaded based on

equal protein content, about 10-20 µg for WCL, and 2-5 µg for EVs. In one case, EV lysates were normalized by cell number and a proportional volume of lysate was loaded to illustrate the magnitude associated with the shift in EV biogenesis and cargo sorting. The separated proteins within the SDS gel were then transferred onto a 0.42 µm PVDF membrane. Membranes were blocked with 5% bovine serum albumin (Sigma) in TBST (19 mM Tris Base, 2.7 mM KCl, 137 mM NaCl, and 0.5 % Tween-20) for 1 h. Membranes were then incubated with the indicated primary antibodies overnight at 4°C with gentle rocking. Membranes were then washed three times with TBST for a total of 15 minutes and incubated with1:5000 HRP conjugated secondary anti-mouse (7076S) and anti-rabbit (7074S) antibodies (Cell Signaling Technology) for 1 hour at room temperature with gentle rocking. Membranes were then washed three times with TBST for a total of 30 minutes, after which they were exposed to ECL reagent (Pierce) and imaged using photosensitive film. Except for β-Actin (8H10D10), which used a 1:5000 dilution, antibodies EGFR (D38B1), STAT3 (124H6), p-STAT3 S727 (6E4), PTEN (D4.3), total AKT (C67E7), p-AKT S473 (D9E), Ras (3965) and PD-L1 (E1L3N) were used at a 1:1000 dilution and purchased from Cell Signaling Technology. The CD81 antibody was used at 1:5000 dilution (R&D Systems, MAB4615).

Flow cytometry & Fluorescence activated cell sorting (FACS)

To compare PD-L1 surface levels in isogenic glioma cell lines with or without PTEN expression, cells were seeded at 5 x 10^5 cells in 10 cm tissue culture treated dishes (Corning). Cells were treated with IFN-γ (50 ng/ml) or PBS as the vehicle control for 24 hours. Cells were washed once with PBS and incubated with 3 mL of TrypLE (Gibco) for 3-5 min or until cells lifted off from the plates with gentle tapping. Cells were then treated with 7 mL of ice cold PBS, collected into 15 mL conical

tubes, and centrifuged at 200 x g for 5 min at 4°C. Cells were resuspended in ice cold FACS buffer (5% BSA, 2 mM EDTA, 1% FBS in PBS) supplemented with 1:100 PE conjugated PD-L1 (eBioscience, MIH1) or PE conjugated Mouse IgG1 kappa Isotype Control (P3.6.2.8.1) and incubated on ice for 30 min. Cells were washed twice using ice cold PBS followed by centrifugation at 200 x g at 4°C and then fixed with 4% paraformaldehyde in PBS for 15 min. Cells were then washed twice by the addition of copious amounts of ice cold PBS and centrifugating as before. Flow cytometry was performed on a ThermoFisher Attune NxT instrument.

Semi-stable NFAT luciferase expressing Jurkat cells both pLJM1-empty, and pLJM1-PD-1, were subjected to fluorescent activated cell sorting (FACS) to sort cells for PD-1 expression. Cells were spun down at 400 x g for 5 min. Cells were resuspended in ice cold FACS buffer containing a 1:100 dilution of FITC conjugated PD-1 antibody (e-bioscience, MIH4), 1:500 fixable cell viability dye (e-bioscience, L34963) and incubated on ice for 30 minutes. Cells were washed by adding excess amounts of ice-cold PBS followed by centrifugation at 400 x g for 5 min. This was repeated one more time and the resulting cell pellet was resuspended in FACS buffer. Stained cells were then sorted on a Sony MA900 with a 100 µm nozzle. Our gating strategy used empty vector Jurkat cells as a negative control for PD-1. To gate live/dead cells, a heated sample of Jurkat cells (1 hour at 65°C) was used as a positive control. Jurkat cells were sorted into RPMI containing 50% FBS and 1x Pen/Strep. Sorting was stopped once 500,000 events were reached.

EV treatment of Jurkat NFAT luciferase reporter cell lines to measure TCR signaling

FACS sorted Jurkat cells expressing the NFAT luciferase reporter, with or without PD-1 expression (Jurkat^{PD-1} and Jurkat^{Ctrl}, respectively), were used to measure the impact EV associated PD-L1 on T

cell receptor (TCR) signaling. Three different EV doses were used to treat Jurkat cells in triplicate (3×10^4 cells/well). For U251 cells, an EV treatment of (++++) corresponds to the total vesicles that originated from one confluent 10 cm dish of cells, or about 3.8×10^6 cells and 2.5×10^9 EV particles being distributed across three triplicate wells or 9×10^4 Jurkat cells. The two other EV doses, (++) and (+), are serially diluted by 1:2. For U87 cells, a dose of (++++) corresponds to a confluent 10 cm dish, or roughly 2.5×10^6 cells, and translates to about 6.4×10^9 EV particles sourced from PTEN-positive cells and 1.05×10^{10} particles from parental PTEN-negative U87 cells. The two other EV doses, (++) and (+), are serially diluted by 1:2.

All treatments conditions were prepared in advance within an ultra-low attachment 96-well plate (Corning, #3474). Only the inner 60 wells of white 96-well clear bottom plates (Corning, #3610) were used the luciferase related experiments. Control wells contained 25 µL of serum-free RPMI supplemented with 150 ng/mL of αCD3 antibody (eBioscience, OKT3). Experimental wells had 25 µL EVs (suspended in serum-free RPMI containing 150ng/mL of αCD3), sourced from either U87 or U251 cells. The plate was then placed in a 37°C incubator for 30 min prior to the addition of Jurkat cells. Following this step, Jurkat cells were seeded at a concentration of 6×10^5 cells/mL or 30,000 cells per well at 50 µL/well. As such, all treatment groups had a final volume of 75 µL and a final αCD3 antibody concentration within the wells of 50 ng/mL. In some instances, Jurkat^{PD-1} were pre-treated for 30 minutes at room temp with a functional grade anti-PD-1 monoclonal antibody (eBioscience, #J116), to mimic ICI inhibitors, or with a mouse IgG1 kappa Isotype control antibody. Jurkat cells were then incubated in a 37°C incubator for 6 hours, at which point, 70 µL of prepared luciferase substrate mix (Promega) was added to each well and incubated for 5 min at room temperature in the dark. Luminance values were read on a Tecan Spark Cyto plate reader.

Statistical Analysis

Unless otherwise noted, all experiments were performed at least three times and averaged. Experiments where only two conditions existed, a two-tailed student T-test was performed. All other experiments with three or more conditions were analyzed by Two-way ANOVA with Tukey's multiple comparison correction. All error bars represent the standard error margin (SEM). In all analyses, statistical significance was reached if the calculated p-value was > 0.05. Statistical analysis was completed on GraphPad Prism v7.

Bibliography

1. Louis DN, Perry A, Reifenberger G, et al. The 2016 World Health Organization Classification of Tumors of the Central Nervous System: a summary. *Acta Neuropathol*. 2016;131(6):803-820. doi:10.1007/s00401-016-1545-1

2. Stupp R, Mason WP, van den Bent MJ, et al. Radiotherapy plus Concomitant and Adjuvant Temozolomide for Glioblastoma. *New England Journal of Medicine*. 2005;352(10):987-996. doi:10.1056/NEJMoa043330

3. Wei SC, Duffy CR, Allison JP. Fundamental mechanisms of immune checkpoint blockade therapy. *Cancer Discov*. 2018;8(9):1069-1086. doi:10.1158/2159-8290.CD-18-0367

4. Ribas A. Adaptive immune resistance: How cancer protects from immune attack. *Cancer Discov*. 2015;5(9):915-919. doi:10.1158/2159-8290.CD-15-0563

5. Ayers M, Lunceford J, Nebozhyn M, et al. IFN-γ-related mRNA profile predicts clinical response to PD-1 blockade. *Journal of Clinical Investigation*. 2017;127(8):2930-2940. doi:10.1172/JCI91190

6. Ribas A, Wolchok JD. Cancer immunotherapy using checkpoint blockade. *Science (1979)*. 2018;359(6382):1350-1355. doi:10.1126/science.aar4060

7. Hou AJ, Chen LC, Chen YY. Navigating CAR-T cells through the solid-tumour microenvironment. *Nat Rev Drug Discov*. 2021;20(7):531-550. doi:10.1038/s41573-021-00189-2

8. Nixon NA, Blais N, Ernst S, et al. Current landscape of immunotherapy in the treatment of solid tumours, with future opportunities and challenges. *Current Oncology*. 2018;25(5):e373-e384. doi:10.3747/co.25.3840

9. Peng W, Chen JQ, Liu C, et al. Loss of PTEN promotes resistance to T cell–mediated immunotherapy. *Cancer Discov*. 2016;6(2):202-216. doi:10.1158/2159-8290.CD-15-0283

10. Zhao J, Chen AX, Gartrell RD, et al. Immune and genomic correlates of response to anti-PD-1 immunotherapy in glioblastoma. *Nat Med*. 2019;25(3):462-469. doi:10.1038/s41591-019-0349-y

11. Cabrita R, Mitra S, Sanna A, et al. The Role of PTEN Loss in Immune Escape, Melanoma Prognosis and Therapy Response. *Cancers (Basel)*. 2020;12(3):742. doi:10.3390/cancers12030742

12. Chida K, Kawazoe A, Kawazu M, et al. A low tumor mutational burden and PTEN mutations are predictors of a negative response to PD-1 blockade in MSI-H/dMMR gastrointestinal tumors. *Clinical Cancer Research*. 2021;27(13):3714-3724. doi:10.1158/1078-0432.CCR-21-0401

13. Chalhoub N, Baker SJ. PTEN and the PI3-kinase pathway in cancer. *Annual Review of Pathology: Mechanisms of Disease*. 2009;4:127-150. doi:10.1146/annurev.pathol.4.110807.092311

14. Sanchez-Vega F, Mina M, Armenia J, et al. Oncogenic Signaling Pathways in The Cancer Genome Atlas. *Cell*. 2018;173(2):321-337.e10. doi:10.1016/j.cell.2018.03.035

15. Brennan CW, Verhaak RGW, McKenna A, et al. The somatic genomic landscape of glioblastoma. *Cell*. 2013;155(2):462-477. doi:10.1016/j.cell.2013.09.034

16. Maehama T, Dixon JE. The tumor suppressor, PTEN/MMAC1, dephosphorylates the lipid second messenger, phosphatidylinositol 3,4,5-trisphosphate. *Journal of Biological Chemistry*. 1998;273(22):13375-13378. doi:10.1074/jbc.273.22.13375

17. Song MS, Salmena L, Pandolfi PP. The functions and regulation of the PTEN tumour suppressor. *Nat Rev Mol Cell Biol*. 2012;13(5):283-296. doi:10.1038/nrm3330

18. Liu P, Gan W, Chin YR, et al. Ptdins(3,4,5) P3 -dependent activation of the mTORC2 kinase complex. *Cancer Discov*. 2015;5(11):1194-11209. doi:10.1158/2159-8290.CD-15-0460

19. Vanhaesebroeck B, Stephens L, Hawkins P. PI3K signalling: The path to discovery and understanding. *Nat Rev Mol Cell Biol*. 2012;13(3):195-203. doi:10.1038/nrm3290

20. Lin Z, Huang L, Li SL, Gu J, Cui X, Zhou Y. PTEN loss correlates with T cell exclusion across human cancers. *BMC Cancer*. 2021;21(1):1-14. doi:10.1186/s12885-021-08114-x

21. Vidotto T, Melo CM, Castelli E, Koti M, dos Reis RB, Squire JA. Emerging role of PTEN loss in evasion of the immune response to tumours. *Br J Cancer*. 2020;122(12):1732-1743. doi:10.1038/s41416-020-0834-6

22. Martinez-Lage M, Lynch TM, Bi Y, et al. Immune landscapes associated with different glioblastoma molecular subtypes. *Acta Neuropathol Commun*. 2019;7(1):1-12. doi:10.1186/s40478-019-0803-6

23. Hanahan D, Weinberg RA. Hallmarks of cancer: The next generation. *Cell*. 2011;144(5):646-674. doi:10.1016/j.cell.2011.02.013

24. Bonaventura P, Shekarian T, Alcazer V, et al. Cold tumors: A therapeutic challenge for immunotherapy. *Front Immunol*. 2019;10(FEB):1-10. doi:10.3389/fimmu.2019.00168

25. Antunes ARP, Scheyltjens I, Duerinck J, Neyns B, Movahedi K, Van Ginderachter JA. Understanding the glioblastoma immune microenvironment as basis for the development of new immunotherapeutic strategies. *Elife*. 2020;9:1-16. doi:10.7554/eLife.52176

26. Blumenthal DT, Yalon M, Vainer GW, et al. Pembrolizumab: first experience with recurrent primary central nervous system (CNS) tumors. *J Neurooncol*. 2016;129(3):453-460. doi:10.1007/s11060-016-2190-1

27. Trimboli AJ, Cantemir-Stone CZ, Li F, et al. Pten in stromal fibroblasts suppresses mammary epithelial tumours. *Nature*. 2009;461(7267):1084-1091. doi:10.1038/nature08486

28. Conley-LaComb MK, Saliganan A, Kandagatla P, Chen YQ, Cher ML, Chinni SR. PTEN loss mediated Akt activation promotes prostate tumor growth and metastasis via CXCL12/CXCR4 signaling. *Mol Cancer*. 2013;12(1). doi:10.1186/1476-4598-12-85

29. Phillips RJ, Mestas J, Gharaee-Kermani M, et al. Epidermal growth factor and hypoxia-induced expression of CXC chemokine receptor 4 on non-small cell lung cancer cells is regulated by the phosphatidylinositol 3-kinase/PTEN/AKT/mammalian target of rapamycin signaling pathway and activation of hypoxia inducible factor-1α. *Journal of Biological Chemistry*. 2005;280(23):22473-22481. doi:10.1074/jbc.M500963200

30. Simeone P, Bologna G, Lanuti P, et al. Extracellular vesicles as signaling mediators and disease biomarkers across biological barriers. *Int J Mol Sci*. 2020;21(7):1-27. doi:10.3390/ijms21072514

31. Desrochers LM, Bordeleau F, Reinhart-King CA, Cerione RA, Antonyak MA. Microvesicles provide a mechanism for intercellular communication by embryonic stem cells during embryo implantation. *Nat Commun*. 2016;7:11958. doi:10.1038/ncomms11958

32. Latifkar A, Hur YH, Sanchez JC, Cerione RA, Antonyak MA. New insights into extracellular vesicle biogenesis and function. *J Cell Sci*. 2019;132(13):jcs222406. doi:10.1242/jcs.222406

33. Raposo G, Stoorvogel W. Extracellular vesicles: exosomes, microvesicles, and friends. *J Cell Biol*. 2013;200(4):373-383. doi:10.1083/jcb.201211138

34. Hoshino A, Costa-Silva B, Shen TL, et al. Tumour exosome integrins determine organotropic metastasis. *Nature*. 2015;527(7578):329-335. doi:10.1038/nature15756

35. Feng Q, Zhang C, Lum D, et al. A class of extracellular vesicles from breast cancer cells activates VEGF receptors and tumour angiogenesis. *Nat Commun*. 2017;8:14450. doi:10.1038/ncomms14450

36. Gabrusiewicz K, Li X, Wei J, et al. Glioblastoma stem cell-derived exosomes induce M2 macrophages and PD-L1 expression on human monocytes. *Oncoimmunology*. 2018;7(4). doi:10.1080/2162402X.2017.1412909

37. Xu R, Rai A, Chen M, Suwakulsiri W, Greening DW, Simpson RJ. Extracellular vesicles in cancer — implications for future improvements in cancer care. *Nat Rev Clin Oncol*. 2018;15(10):617-638. doi:10.1038/s41571-018-0036-9

38. Ricklefs FL, Alayo Q, Krenzlin H, et al. Immune evasion mediated by PD-L1 on glioblastoma-derived extracellular vesicles. *Sci Adv*. 2018;4(3). doi:10.1126/sciadv.aar2766

39. Chen G, Huang AC, Zhang W, et al. Exosomal PD-L1 contributes to immunosuppression and is associated with anti-PD-1 response. *Nature*. 2018;560(7718):382-386. doi:10.1038/s41586-018-0392-8

40. Parsa AT, Waldron JS, Panner A, et al. Loss of tumor suppressor PTEN function increases B7-H1 expression and immunoresistance in glioma. *Nat Med*. 2007;13(1):84-88. doi:10.1038/nm1517

41. Mittendorf EA, Philips A V., Meric-Bernstam F, et al. PD-L1 expression in triple-negative breast cancer. *Cancer Immunol Res*. 2014;2(4):361-370. doi:10.1158/2326-6066.CIR-13-0127

42. Lastwika KJ, Wilson W, Li QK, et al. Control of PD-L1 expression by oncogenic activation of the AKT-mTOR pathway in non-small cell lung cancer. *Cancer Res*. 2016;76(2):227-238. doi:10.1158/0008-5472.CAN-14-3362

43. Dong Y, Richards JA, Gupta R, et al. PTEN functions as a melanoma tumor suppressor by promoting host immune response. *Oncogene*. 2014;33(38):4632-4642. doi:10.1038/onc.2013.409

44. Song M, Chen D, Lu B, et al. PTEN Loss Increases PD-L1 Protein Expression and Affects the Correlation between PD-L1 Expression and Clinical Parameters in Colorectal Cancer. *PLoS One*. 2013;8(6). doi:10.1371/journal.pone.0065821

45. Hill VK, Kim JS, James CD, Waldman T. Correction of PTEN mutations in glioblastoma cell lines via AAV-mediated gene editing. *PLoS One*. 2017;12(5):1-11. doi:10.1371/journal.pone.0176683

46. Garcia-Diaz A, Shin DS, Moreno BH, et al. Interferon Receptor Signaling Pathways Regulating PD-L1 and PD-L2 Expression. *Cell Rep*. 2017;19(6):1189-1201. doi:10.1016/j.celrep.2017.04.031

47. Hara T, Chanoch-Myers R, Mathewson ND, et al. Interactions between cancer cells and immune cells drive transitions to mesenchymal-like states in glioblastoma. *Cancer Cell*. 2021;39(6):779-792.e11. doi:10.1016/j.ccell.2021.05.002

48. Chen P, Zhao D, Li J, et al. Symbiotic Macrophage-Glioma Cell Interactions Reveal Synthetic Lethality in PTEN-Null Glioma. *Cancer Cell*. 2019;35(6):868-884.e6. doi:10.1016/j.ccell.2019.05.003

49. Ni X, Wu W, Sun X, et al. Interrogating glioma-M2 macrophage interactions identifies Gal-9/Tim-3 as a viable target against PTEN -null glioblastoma. *Sci Adv*. 2022;8(27):5165. doi:10.1126/sciadv.abl5165

50. Zaretsky JM, Garcia-Diaz A, Shin DS, et al. Mutations associated with acquired resistance to PD-1 blockade in melanoma. *New England Journal of Medicine*. 2016;375(9):819-829. doi:10.1056/NEJMoa1604958

51. Tumeh PC, Harview CL, Yearley JH, et al. PD-1 blockade induces responses by inhibiting adaptive immune resistance. *Nature*. 2014;515(7528):568-571. doi:10.1038/nature13954

52. Holz MK, Ballif BA, Gygi SP, Blenis J. mTOR and S6K1 mediate assembly of the translation preinitiation complex through dynamic protein interchange and ordered phosphorylation events. *Cell*. 2005;123(4):569-580. doi:10.1016/j.cell.2005.10.024

53. Andreola G, Rivoltini L, Castelli C, et al. Induction of lymphocyte apoptosis by tumor cell secretion of FasL-bearing microvesicles. *Journal of Experimental Medicine*. 2002;195(10):1303-1316. doi:10.1084/jem.20011624

54. Taylor DD, Lyons KS, Stanson J, Whiteside TL. T-Cell Apoptosis and Suppression of T-Cell Receptor / CD3- ζ by Fas Ligand-Containing Membrane Vesicles Shed from Ovarian Tumors. *Clinical Cancer Research*. 2003;9(502):5113-5119.

55. J. Klibi, T. Niki, A. Riedel, C. Pioche-Durieu, S. Souquere, E. Rubinstein, S. Le Moulec, J. Guigay, M. Hirashima, F. Guemira, D. Adhikary, J. Mautner PB. Blood diffusion and Th1-suppressive effects of galectin-9 containing exosomes released by epstein-barr virus-infected nasopharyngeal carcinoma cells. (Blood (2009) 113, 9 (1957-1966)). *Blood*. 2009;114(18):3974. doi:10.1182/blood-2008-02- 142596

56. Lee MF, Trotman LC. PTEN: Bridging Endocytosis and Signaling. *Cold Spring Harb Perspect Med*. Published online 2019:a036103. doi:10.1101/cshperspect.a036103

57. Abe N, Inoue T, Galvez T, Klein L, Meyer T. Dissecting the role of PtdIns(4,5)P2 in endocytosis and recycling of the transferrin receptor. *J Cell Sci*. 2008;121(9):1488-1494. doi:10.1242/jcs.020792

58. Kadri S, Nakada-Tsukui K, Watanabe N, Jeelani G, Nozaki T. PTEN differentially regulates endocytosis, migration, and proliferation in the enteric protozoan parasite Entamoeba histolytica. *PLoS Pathog*. 2022;18(5). doi:10.1371/journal.ppat.1010147

59. Basquin C, Malardé V rie, Mellor P, et al. The signalling factor PI3K is a specific regulator of the clathrin-independent dynamin-dependent endocytosis of IL-2 receptors. *J Cell Sci*. 2013;126(5):1099-1108. doi:10.1242/jcs.110932

60. Gozzelino L, De Santis MC, Gulluni F, Hirsch E, Martini M. PI(3,4)P2 Signaling in Cancer and Metabolism. *Front Oncol*. 2020;10(March):1-12. doi:10.3389/fonc.2020.00360

61. De Craene JO, Bertazzi DL, Bär S, Friant S. Phosphoinositides, major actors in membrane trafficking and lipid signaling pathways. *Int J Mol Sci*. 2017;18(3). doi:10.3390/ijms18030634

62. Behnia R, Munro S. Organelle identity and the signposts for membrane traffic. *Nature*. 2005;438(7068):597-604. doi:10.1038/nature04397

63. Naguib A, Bencze G, Cho H, et al. PTEN functions by recruitment to cytoplasmic vesicles. *Mol Cell*. 2015;58(2):255-268. doi:10.1016/j.molcel.2015.03.011

64. Miranda AM, Lasiecka ZM, Xu Y, et al. Neuronal lysosomal dysfunction releases exosomes harboring APP C-terminal fragments and unique lipid signatures. *Nat Commun*. 2018;9(1). doi:10.1038/s41467-017-02533-w

65. Hessvik NP, Øverbye A, Brech A, et al. PIKfyve inhibition increases exosome release and induces secretory autophagy. *Cellular and Molecular Life Sciences*. 2016;73(24):4717-4737. doi:10.1007/s00018-016-2309-8

66. Sanjana NE, Shalem O, Zhang F. Improved vectors and genome-wide libraries for CRISPR screening. *Nat Methods*. 2014;11(8):783-784. doi:10.1038/nmeth.3047